Journal of Applied Geophysics 91 (2013) 49–65

Contents lists available at SciVerse ScienceDirect

Journal of Applied Geophysics

journal homepage: www.elsevier.com/locate/jappgeo

Non-invasive characterization of water-bearing strata using a combination of geophysical techniques

Jun Lin [a], Tingting Lin [a,*], Yanju Ji [a], Zubin Chen [a], Yiping Zhao [b], Haisheng Li [b]

[a] College of Instrumentation and Electrical Engineering, Jilin University, Changchun 130061, China
[b] Graduate School of the Department of Water Resources, Inner-Mongolia 010020, China

ARTICLE INFO

Article history:
Received 1 July 2012
Accepted 7 February 2013
Available online 16 February 2013

Keywords:
Groundwater
Fault
2D seismic
Electrical method
Magnetic resonance sounding

ABSTRACT

Hydrogeological investigations were carried out in an arid area of Inner-Mongolia to determine the locations of future water supply resources. The first geophysical survey was conducted near Baiqi to identify favorable boreholes using magnetic resonance sounding (MRS). The yield capacities of 43 sites were investigated, and the extent of the potential groundwater storage was determined. Previous studies have indicated that a major tectonic structure may have a significant impact on the groundwater flow and well yield in the study area. Therefore, high-resolution seismic surveys were applied in the second stage of the investigation to determine the fault locations. After the regional identification, a major structure was investigated in detail to map the fracture patterns. Based on the assumption that the hydraulic conductivity of this formation is similar along the entire strike of the fracture, we proposed drilling a borehole (BQ3) in the zone. However, this well has a yield of only 0.8 L/s, falling short of the required flow rate of 3.0 L/s. Therefore, the objective of the final stage of exploration was to accurately define the attitude and extension of the aquifer and to select a more favorable borehole site that would meet the required water flow rate. The geophysical exploration was carried out using time-domain electromagnetic (TDEM) and MRS methods. The MRS results suggest optimal locations for water supply boreholes within the subsurface structures mapped by the TDEM inversion method. The data obtained by drilling and coring are in agreement with the predicted aquifer thickness from the TDEM data. Pumping tests indicate that the water discharge of borehole BQ4 was 3.5 L/s. Our results demonstrate that the delineation of the groundwater body using a combined application of three geophysical methods (the MRS, TDEM and 2D seismic methods) was successful.

1. Introduction

The effective management of groundwater resources is of paramount importance in many regions of the world, particularly for those regions that suffer from a lack of fresh surface water and insufficient rainfall. The town of Baiqi in the Chinese province of Inner-Mongolia is typical of such areas, the average annual precipitation is 350.1 mm and groundwater is the only source of fresh water (Liu and Xia, 2004; Liu et al., 2005).

In the 1950s, various geophysical methods and borehole data were used to understand the geophysical features of the area. Consequently, the orientation of the faults within the study area was found to be predominantly ENE–WSW (faults F1 and F2) and E–W (Faults F3 and F4 in Fig. 1). A magnetic resonance sounding (MRS) survey was conducted in Baiqi in May 2002, in response to the request of the Inner-Mongolian government for comprehensive groundwater mapping and water supply planning. Forty-three sites were investigated using MRS, and the potential high groundwater storage area was identified (Fig. 1). There is an artesian well (BQ1) located near fault F1, suggesting that the fractures and faults may form an important groundwater resource in this area. Further, combined methods should be used to optimize the locations of further water supply boreholes within this complex terrain.

The accurate determination of fracture locations would provide important information on groundwater resources. For example, high-resolution reflection method has been developed and used for geotechnical, environmental and groundwater-related studies (Myers et al., 1987; Shtivelman and Goldman, 2000; Shtivelman et al., 1998). However, the method cannot yet predict groundwater locations or estimate total groundwater amounts.

Considering the depths and electrical resistivities of aquifers, MRS is a promising electromagnetic method. It allows for the direct detection of aquifers by assessing the groundwater, as opposed to detecting the electrical properties of the sediments (Jiang et al., 2011a,b; Schirov et al., 1991; Yaramanci et al., 1999). Furthermore, this method can estimate the water content, hydraulic conductivity, transmissivity, and storage-related properties (Lachassagne et al., 2005). The main geophysical constraint for MRS applications is the low level of the MRS

* Corresponding author at: College of Instrumentation and Electrical Engineering, Jilin University, No. 938 Ximinzhu Avenue, Changchun, Jilin, China. Tel./fax: +86 431 88502473.
E-mail address: ttlin@jlu.edu.cn (T. Lin).

0926-9851/$ – see front matter © 2013 Elsevier B.V. All rights reserved.
http://dx.doi.org/10.1016/j.jappgeo.2013.02.002

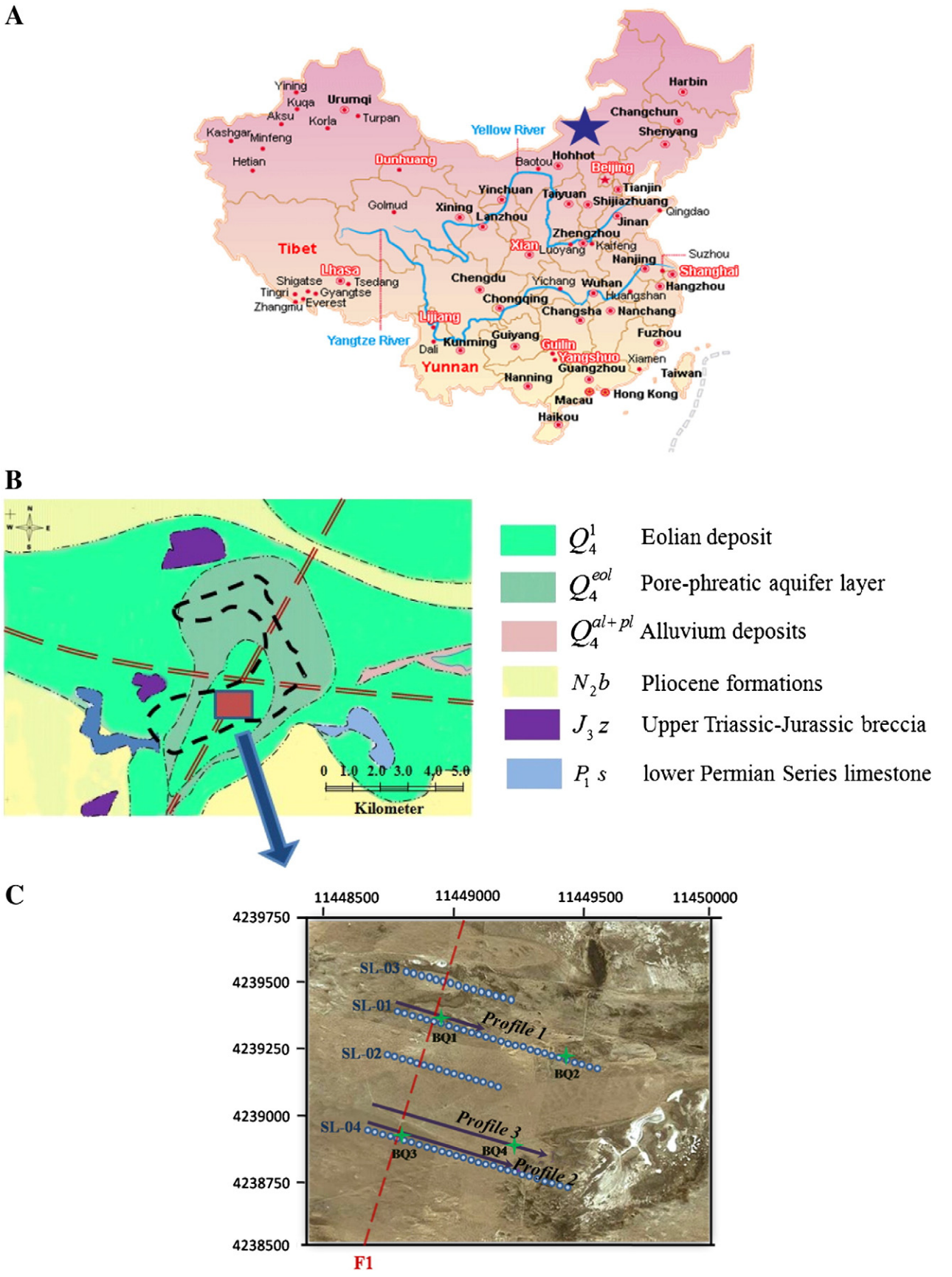

Fig. 1. Location and geological map of the survey area. (A) Maps showing Baiqi (blue star), where geophysical exploration was carried out in 2002. (B) The simplified geological map of the survey area, and an enlarged aerial photo of the exploration site. The black dotted line indicates 43 MRS testing sites, and the potential high groundwater storage area is shown in brown. (C) The locations of the seismic lines (SL), TDEM Profiles, and boreholes BQ1, 2, 3 and 4 are indicated.

signal the groundwater body produces compared to the electromagnetic noise at the Larmor frequency f_0 specified for the measurements (Plata and Rubio, 2002). Furthermore, the instrument for MRS has been designed to investigate groundwater up to 150 m; information on the deeper parts of the aquifer cannot be acquired by current commercially available MRS equipment.

The main objectives of the investigation are as follows: 1) to describe the general trend of the main faults in this complex area by using high resolution seismic reflection method with a view of improving our knowledge of their general geometry and structure; 2) to investigate the efficiency of using MRS to define and characterize water bearing geological formations according to their hydraulic and storage related properties within the fracture zone; 3) to explore the advantages of the QT inversion model (Mueller-Petke and Yaramanci, 2010) as well as the joint inversion model in distinguishing aquifer layers by combing MRS and TEM within different MRS signal-to-noise conditions; and 4) to develop a conceptual model of groundwater flow in the study area from the results of several geophysical methods.

Many researchers have used the MRS, TDEM, and seismic methods separately in hydrology studies (Burazer et al., 2010; Girard et al., 2007; Porsani et al., 2012), or using MRS and TEM joint together for delineating salt water and fresh aquifers (Legchenko et al., 2009). However, there is limited record to our knowledge of integrating the three methods together for the groundwater data interpretations. Importantly, distinct MRS inversion schemes were chosen in this study according to different MRS signal-to-noise ratios. And we compared the joint inversion of MRS and TEM methods with the QT inversion model at noisier place. In this study, we first present the geological and hydrogeological features of the study area and then explain the data acquisition techniques (TDEM, 2D seismic, and MRS), processing methods, and the physical properties of the drilled formations. Finally, we explain the results from the combined technologies.

2. Site description

2.1. Physical environment

Baiqi has an area of 6.23 km^2 and is located at the center of Inner-Mongolia, China, with a latitudinal extent between 42° 05′ and 43° 15′ and a longitudinal extent between 114° 05′ and 115º 37′. Baiqi has a semiarid continental climate. Its population is about 0.7 million. Approximately 9.8% of the town is cultivated; 33.3% is covered by meadow and sandhills; and 10.2% consists of heathlands, marshlands, bogs and deciduous or coniferous forests. Urban areas occupy 14.2% of Baiqi, and uncultivated land covers the remaining 32%. Approximately 25% of Inner-Mongolia province has access to drinking water via shallow wells (3–6 m deep) and boreholes (20–50 m deep), which are mostly equipped with hand pumps. Seventy-five percent of the population in Baiqi does not have access to drinking water.

2.2. Hydrogeological environment of the study area

In this section, based on the reports and information from the Water Resources Survey of Inner-Mongolia, we briefly describe some of the dominant geological features of the study area.

The survey area is topographically flat and its altitude from the sea level decreases smoothly from the north to the south. Much of the study area is covered by Quaternary eolian deposits, some of which have been affected by soil salination (Liu et al., 2007). Due to the low intensity and variability, Quaternary eolian deposits are not considered reliable for groundwater storage or the renewal of groundwater resources. The Quaternary pore-phreatic aquifer layer is alternating with the eolian deposits in the middle part of the study area. In the study area, Cretaceous Bahuayan unit (a mixture of marl, sand and gravels and quartizite) is overlain with Neogene formations, consisting of consolidated sandstone, mudstone and clay. Conglomerates are also present, albeit to a lesser extent. Confined aquifers are assumed to be in the Bahuayan unit, whereas Neogene formations are considered to be aquicludes, as they rarely possess hydraulic conditions that are suitable for an aquifer. The Jurassic Zhangjiajie breccia and lower Permian Series limestone are also found in this area. However, they are believed to be heterogeneous aqueous systems.

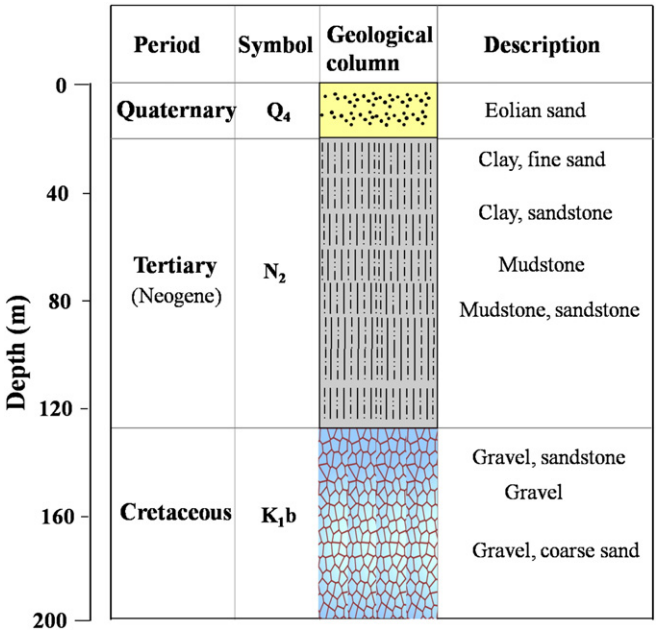

Fig. 2. Lithological description of water well BQ1.

In this region, the groundwater is frequently used for irrigation from deep wells that penetrate tens of meters into the fractured layers with high flow rates. A simplified geological column of the survey area is presented for the well log from BQ1 (Fig. 2).

3. Geophysical data acquisition

3.1. Seismic data acquisition

High-resolution seismic reflection data were collected along 4 lines across fracture F1. The data were originally acquired along the 1500-m-long line SL-01, which runs perpendicular to the scarp and passes through the artesian well BQ1. After the analysis of line SL-01, additional data were acquired along lines SL-02, SL-03 and SL-04. All of the lines are parallel to SL-01 and were positioned to determine the width of the fault zone in the shallow subsurface.

Pre-production tests, commonly known as walkaway noise tests, allow for the selection of an optimal recording window and for the determination of recording parameters. The walkaway noise tests, conducted prior to the acquisition of all the lines, were used to determine the minimum and maximum shot-to-receiver distances, receiver type, shot and receiver spacing, energy source type, and pre-A/D (analog-to-digital) filter settings. High-frequency sources and receivers

Table 1
Methods, equipments and interpretation tools.

Methods	Array	Equipment	Interpretation tools
Seismic	CDP:10 m	Summit (Germany)	Geogiga Interpretation Software
TDEM	Tx/Rx:100×100 m	ATEM-II (Jilin University)	ATEM-II software (Ji et al., 2003)
MRS	Tx/Ri: 100×100 m and 150×150 m	NUMIS (IRIS instrument)	"Samovar_01" software (Legchenko and Shushako, 1998)

Table 2
Seismic data acquisition: equipment parameters.

Recorder	48 channel Summit seismograph
Energy source	Dynasource
Receivers—double geophones	100 Hz
Receiver spacing	5.0 m
Shot spacing	5.0 m (every station)
Shot location	Near 1st receiver (off-end geometry)
Maximum fold	24
Time sampling interval	0.5 ms
Analog band-pass filters	8.7–180 Hz
Record length	0.5 s

are critical in high-resolution studies. The seismic energy was provided by a 50-caliber rifle attached to a steel plate, which allowed the muzzle to be lowered 0.6 m below the ground surface into an augered hole. Firing a gun in a borehole diminishes the effects of air-coupled waves and increases the amplitude and dominant frequency of the recorded seismic energy. Two 100-Hz geophones, connected in series and spaced 0.6 m parallel to the direction of the wind, were used for each channel. The two-geophone array helped increase the signal amplitude and attenuate the wind noise.

A 24-channel Summit seismic recording system (Input/Output, Inc., Germany) was used to amplify, filter, and convert the data from analog to digital. Analog band-pass 8.7–180 Hz filters enhanced the data bandwidth by decreasing the amplitudes of the low and high frequency noise. This further increases the incoming post-filter signals (Jiang et al., 2006). The data were plotted over 0.400 s time windows. The equipment and parameters used in the survey are listed in Table 2.

3.2. TDEM data acquisition

TDEM has been used in a wide variety of hydrogeological and environmental problems and has proven to be efficient. The measured voltages are usually converted to apparent resistivities, that are easy to interpret (Fitterman and Steward, 1986; Kafri and Goldman, 2005). The delay time (t) is related to the induced voltage by the following expression:

$$\rho_a = \frac{\mu_0}{4\pi t}\left[\frac{2\pi\mu_0 a^2 \mathrm{SrI}}{5tV}\right]^{2/3} \quad (1)$$

where μ_0 is the magnetic permeability, a is the radius of transmitter loop, Sr is the area of receiving coil, I is the transmitting current, t is the delay time, and V is the voltage induced in the receiver coil.

The TDEM method can be used for vertical sounding or profiling. Some sounding curves were intentionally located near the water wells or the MRS test sites, for correlating between the formation resistivity and lithology, or providing resistivity for the MRS–TEM joint inversion schemes. Most of the other soundings were carried out along the profiles to provide a general view of the electrical resistivity distribution in the fracture zones, identified by the seismic survey. Five stations were installed near seismic line 01, whereas eight stations were installed near seismic line 04 (Fig. 1). The data were acquired using the ATEM-II equipment, developed at Jilin University, China and used the coincident loop configuration (Ji et al., 2006). The loop sides were 100 m long, and the acquisition times were 5–130 μs at a frequency of 25 Hz. A transmitter current of 8–13 A was used.

Table 3
MRS relaxation times measured for different rocks.

Rock type	Decay time (ms)
Clay bound water	$T_2^*<3$
Sandy clays	$T_2^*<30$
Clay sands, very fine sands	$30<T_2^*<60$
Fine sands	$60<T_2^*<120$
Medium sands	$120<T_2^*<180$
Coarse sands	$180<T_2^*<300$
Gravel deposits	$300<T_2^*<600$
Fractured limestone	$600<T_2^*<800$
Karst limestone	$800<T_2^*<1000$

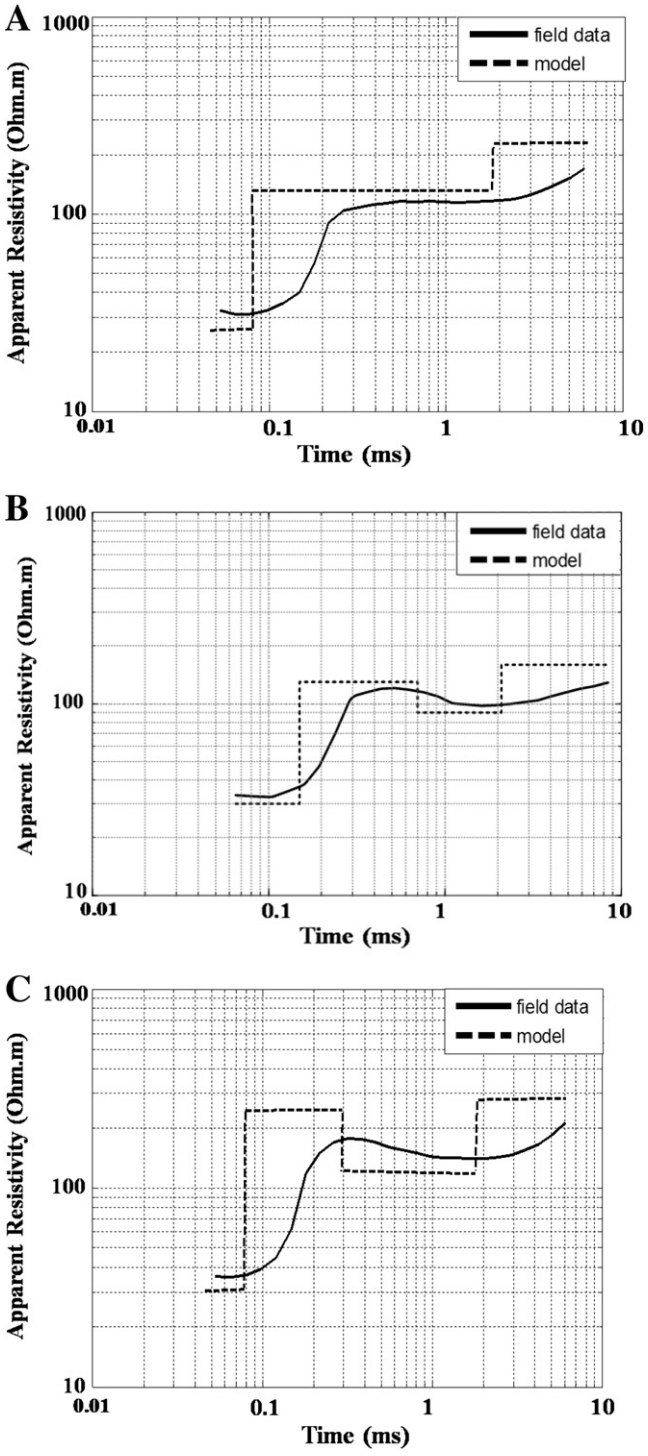

Fig. 3. Apparent resistivity curve was calculated from the field data, and TDEM initial model was obtained by the inversion process for each site. (A) BQ2 (MRS sounding site); (B) BQ3 (MRS sounding site); (C) BQ4 (MRS sounding site).

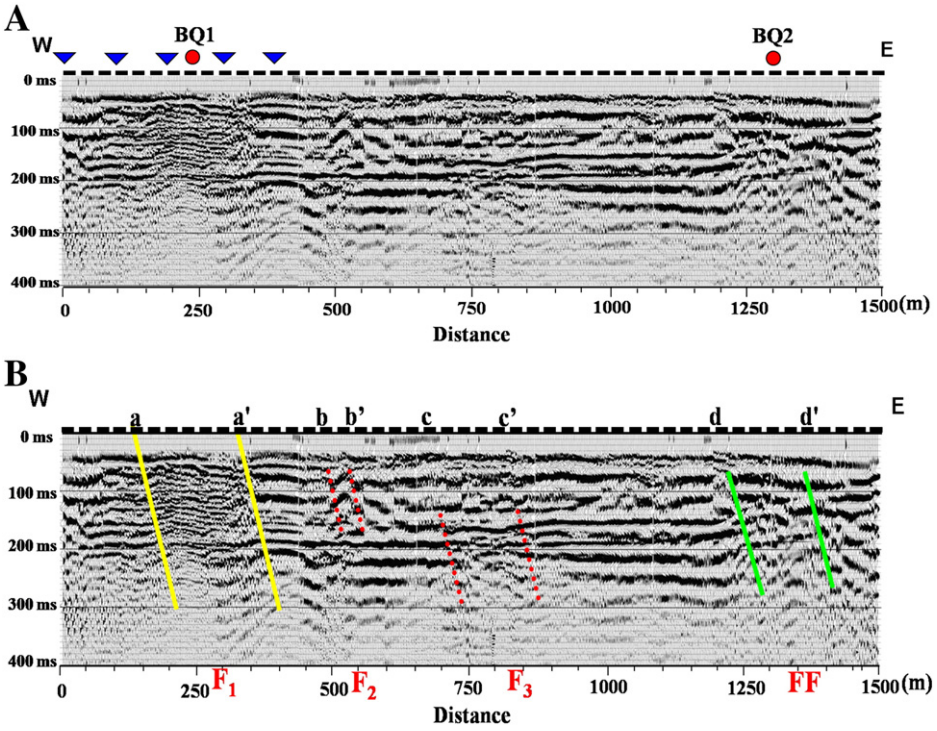

Fig. 4. Seismic sections along line SL-01. (A) Seismic reflection sections; (B) interpreted seismic reflection sections. The blue triangles denote the TDEM sounding sites of profile-RL1; the red circles denote the well locations of BQ1.

3.3. Magnetic resonance sounding method

The MRS method has been described earlier by Legchenko and Valla (2002), Lubczynski and Roy (2003) and Yaramanci (2004). During the 2002 survey, the NUMIS^{plus} MRS system was used with a coincident Tx/Rx loop configuration. In addition to the 43 sites, the new locations of the MRSs were selected based on the integration of high resolution seismic line and the TDEM resistivity map (Table 1).

In our study, the geomagnetic field in the three study areas had an inclination of 39°, and the field intensity varied between 55,732 and

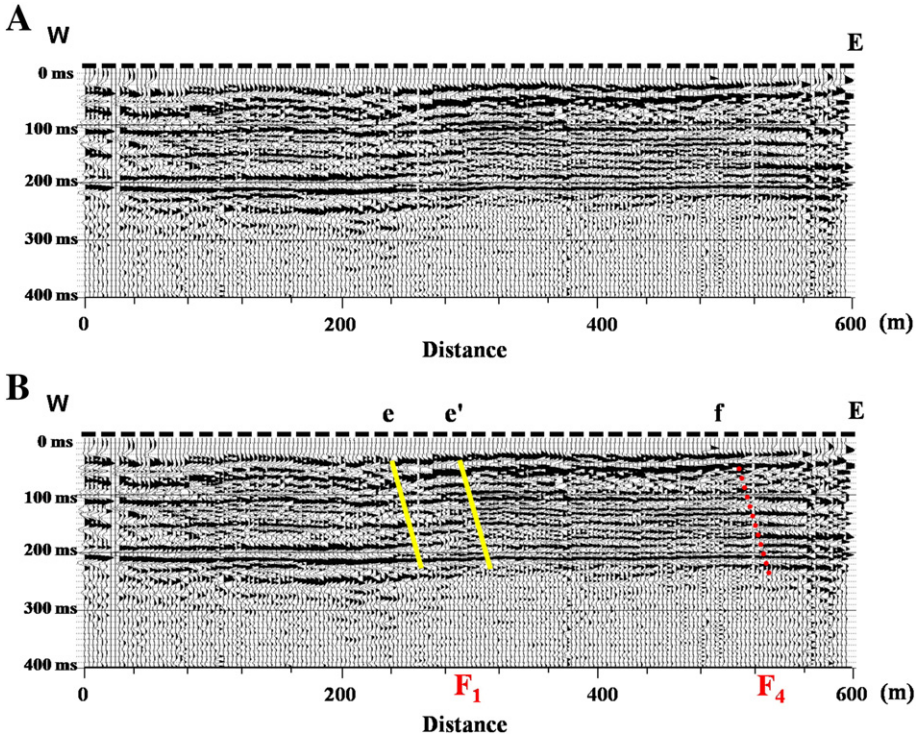

Fig. 5. Seismic sections along line SL-02. (A) Seismic reflection sections; (B) interpreted seismic reflection sections.

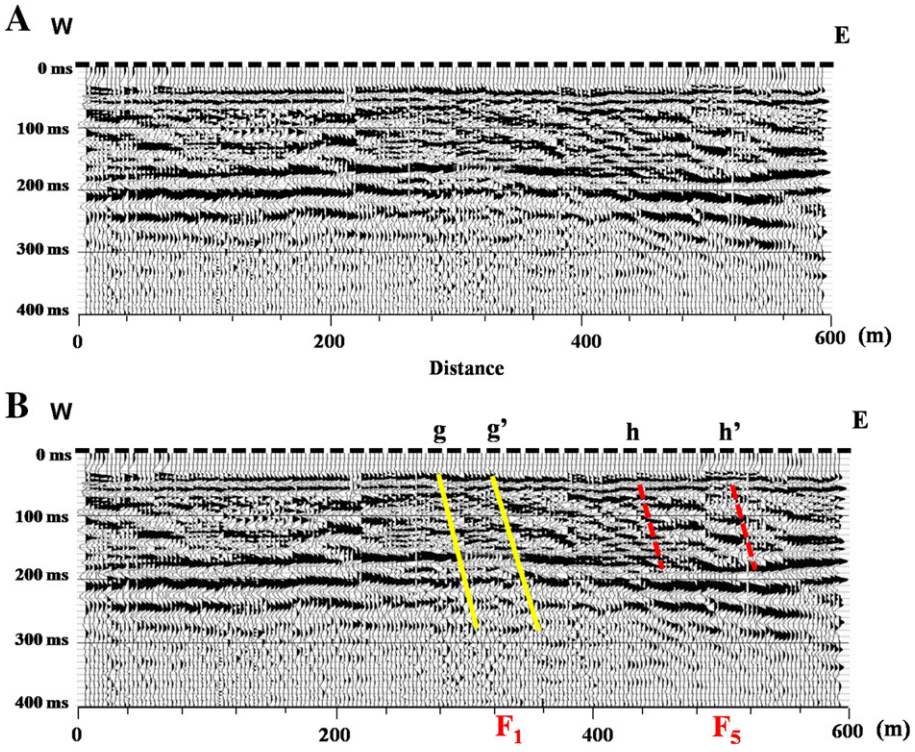

Fig. 6. Seismic sections along line SL-03. (A) Seismic reflection sections; (B) interpreted seismic reflection sections.

56,017 nT, equivalent to a Larmor frequency of 2372 to 2385 Hz. Due to the low noise level in the study area, a square loop was typically used with 64–100 stackings.

The geophysical parameters obtained using MRS include the MRS water content (W_{MRS}) and the relaxation times (T_2^*), which are linked to the mean size of the water-bearing pores. The typical values of T_2^* for the different lithology classes are listed in Table 3.

To calculate the intrinsic permeability of rocks, Legchenko et al. (2004) proposed the following equations for sandy aquifers:

$$K_{MRS} = C_p w T_1^{\,2} \tag{2}$$

$$T_{MRS} = K_{MRS} \Delta z \tag{3}$$

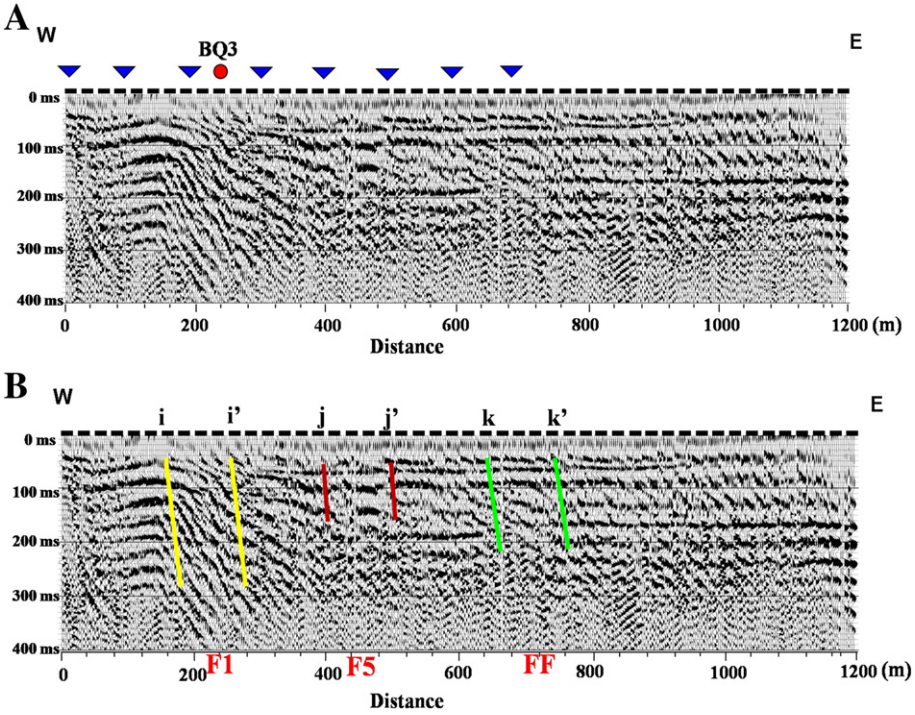

Fig. 7. Seismic sections along line SL-04. (A) Seismic reflection sections; (B) interpreted seismic reflection sections. The blue triangles denote the TDEM sounding sites of profile-RL2; the red circles denote the well locations of BQ3.

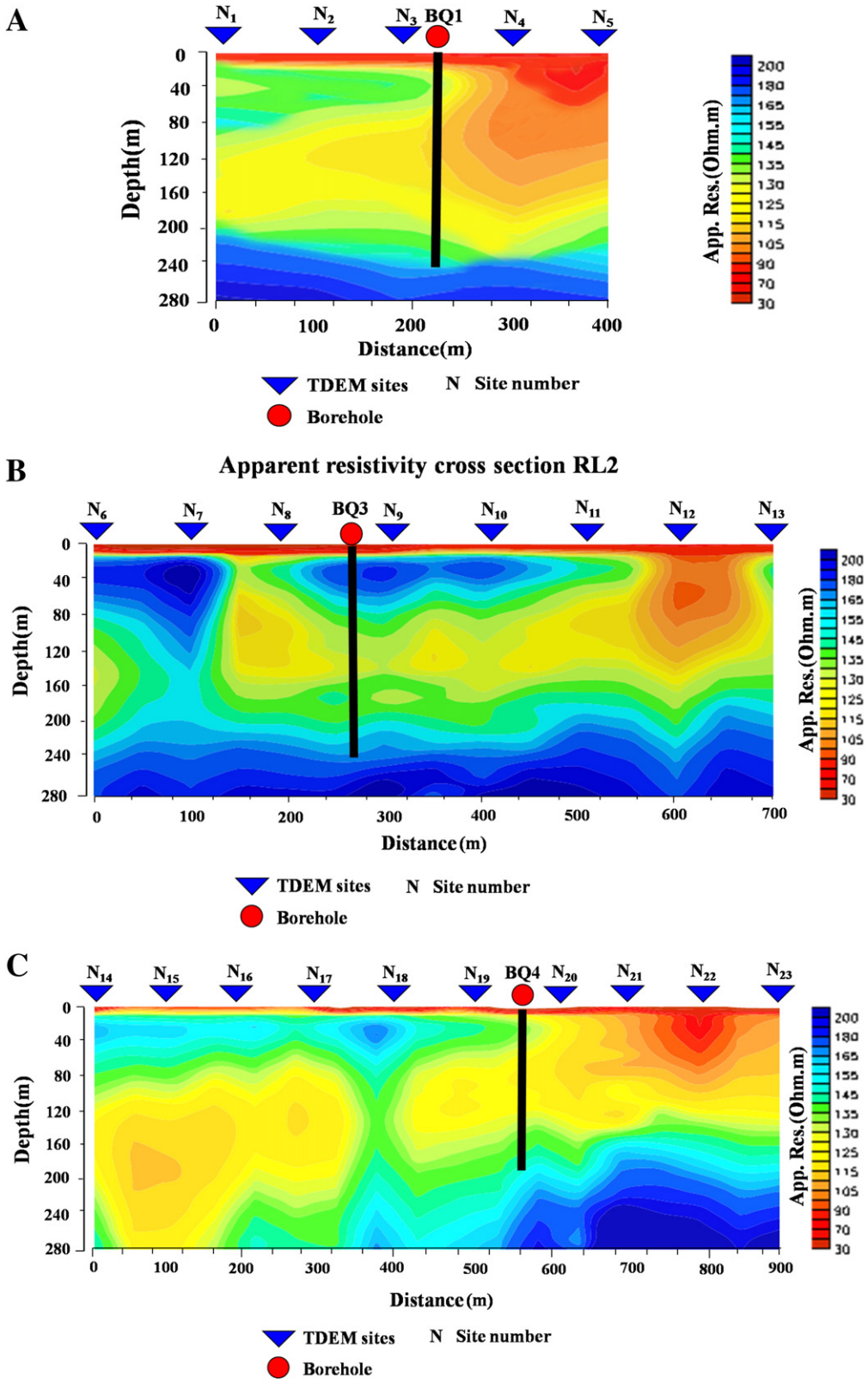

Fig. 8. Profiles of the apparent resistivities with depth. (A) Profile-RL1, generated by contouring 5 TDEM soundings in the area, shows resistivity vs. depth. (B) Profile-RL2, generated by contouring 8 TDEM soundings in the area, showing resistivity vs. depth. (C) Profile-RL3, generated by contouring 10 TDEM soundings in the area, showing resistivity vs. depth.

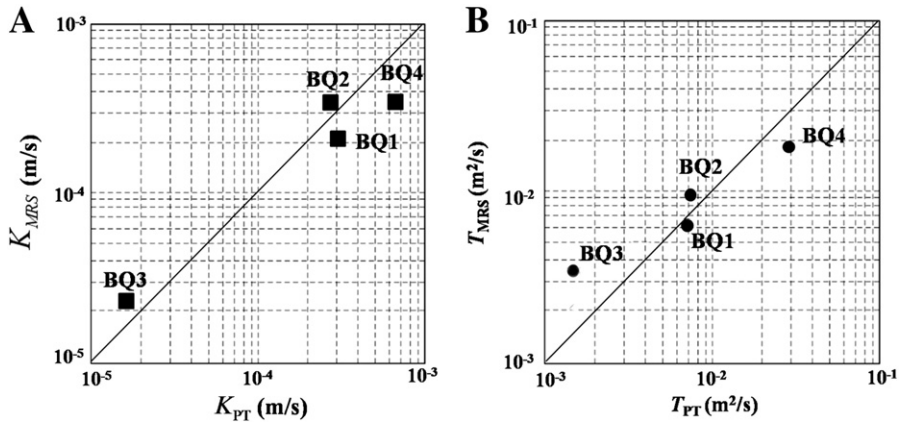

Fig. 9. MRS parameters vs. local aquifer conductivity (A) and transmissivity (B).

Table 4
Comparison of MRS parameters with the pumping test results.

	Pumping tests				MRS			
	Q_{PT} (10^{-3} m³/s)	T_{PT} (10^{-3} m²/s)	K_{PT} (10^{-4} m/s)	q_{PT} (L/s·m)	Q_{MRS} (10^{-3} m³/s)	T_{MRS} (10^{-3} m²/s)	K_{MRS} (10^{-4} m/s)	S/N
BQ1	6.94	6.90	2.30	2.4	6.11	6.61	2.26	11.30
BQ2	9.72	8.81	2.93	2.7	11.4	9.95	3.30	4.51
BQ3	2.32	1.23	0.11	0.8	1.88	2.45	0.19	3.77
BQ4	16.11	15.85	5.01	3.5	15.75	12.77	2.66	8.68

where Δz is the thickness of a water-saturated layer and K_{MRS} and T_{MRS} are the MRS hydraulic conductivity and transmissivity, respectively. T_1 represents the longitudinal relaxation time; C_p is a parametric factor derived from the pumping test and hydraulic conductivity K_{PT} data according to the relation:

$$C_p = T_{PT} \Big/ \sum_{i=1}^{N} w_i T_{1i}^2 \Delta z_i, \tag{4}$$

for the i-th water-saturated layer (Nielsen et al., 2011).

Additionally, the hydraulic conductivity (K) in confined water can also be calculated by the single-well Dupuit steady-flow formula:

$$K = \frac{0.366(\log R - \log r)Q}{\Delta z S_w} \tag{5}$$

where R is the influence radius following the empirical formula:

$$R = 10 S_w \sqrt{K} \tag{6}$$

where S_w is the designed drawdown, r is the well size, and Q is the water inflow during the designated unit of time. Through an iteration process, we can finally get the solution of R and K by combining Eqs. (5) and (6). Additionally, based on Eq. (4) and an assumed drawdown and well size, the MRS water inflow Q_{MRS}, can be estimated using the MRS hydraulic conductivity K_{MRS}:

$$Q_{MRS} = \frac{K_{MRS} \Delta z S_w}{0.366(\log R - \log r)}. \tag{7}$$

4. Interpretation techniques

4.1. TDEM inversion methodology

The TDEM method was interpreted by a widely used inversion method, the singular value decomposition (SVD), as described by Raiche et al. (1985). The iterations are terminated when the error between the two adjacent iterations has not changed significantly or the maximum number of iterations has been reached.

The log–log plots of apparent resistivity versus time and interpreted models of BQ2, BQ3 and BQ4 are shown in Fig. 3, respectively. The fit between the measured data and the calculated data is very good with RMS error <2%. Three layers of different resistivity were inverted at the vicinity of boreholes BQ2 and BQ3, whereas four layers were used at the vicinity of borehole BQ4. Thus, the geological data from the boreholes located close to TDEM the measuring sites are very important constraint for the inversion.

4.2. MRS inversion methodology

Legchenko (2006) defines a lower limit of signal-to-noise ratio of 2 (S/N > 2) for reliable interpretation of the MRS data. Due to the equivalence, several models can fit the data (Mohnke and Yaramanci, 2002). For accurate modeling, the kernel function was calculated based on the electrical model of the subsurface layer that was inverted by TDEM. The regularization parameter controls the smoothness of the interpreted free water content as a function of depth. Blocky inversion was controlled with interpretation steps by the TDEM model geometry. Thus, in this model, the coupled layer thicknesses by the two methods are then altered to improve the model fit.

Fig. 10. The MRS and TDEM inversion results at BQ2 site: (A) the measured MRS signal and calculated smooth inversion and QT model signals. SNR denotes signal to noise ratio. (B) Water content and decay time inverted by smooth and blocky inversions and the TDEM inversion result at the MRS sounding sites. (C) The QT inversion results and the nearby borehole data. PWC denotes the partial water contents.

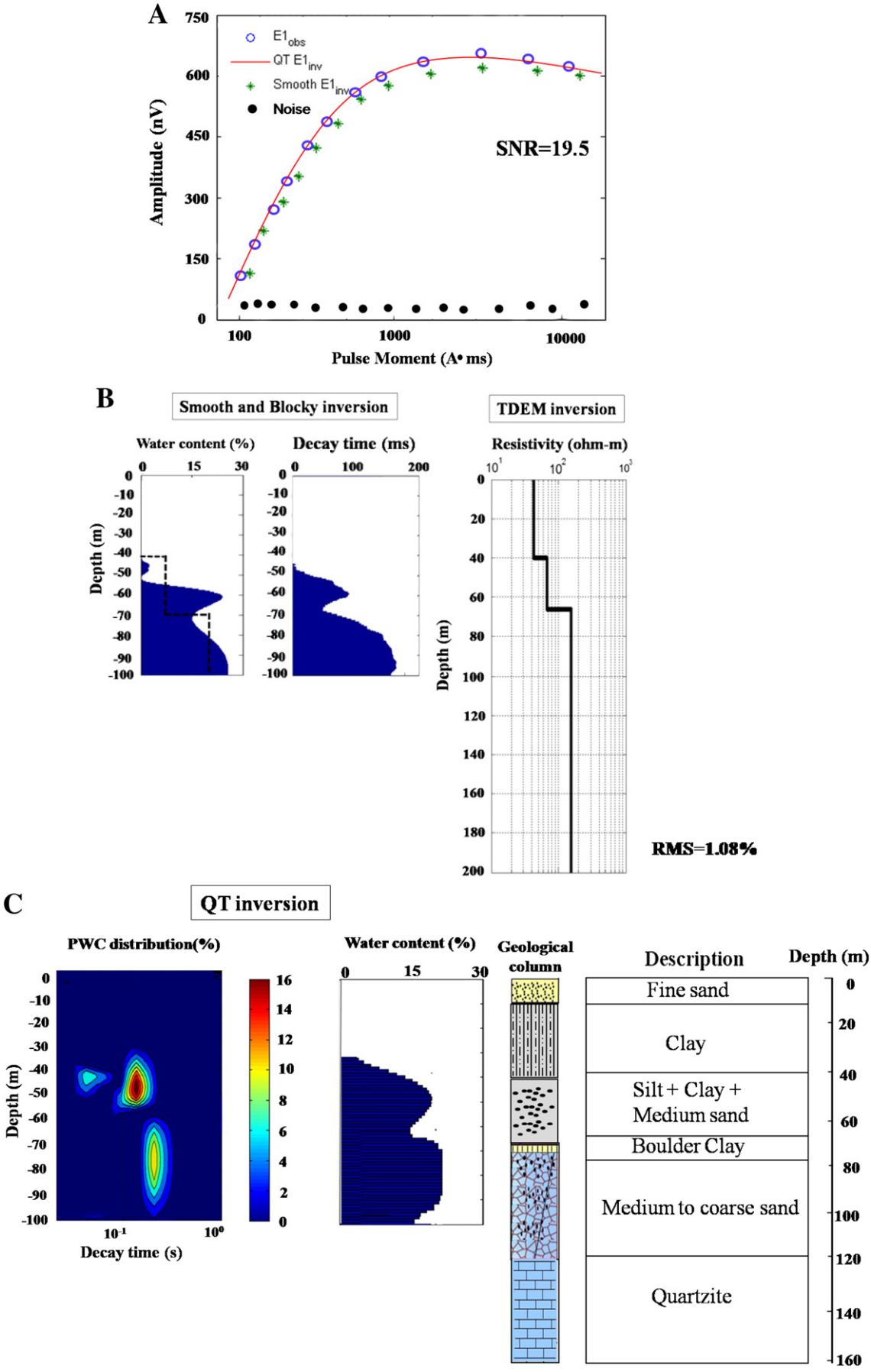
A
E1obs
QT E1inv
Smooth E1inv
Noise
SNR=19.5
Amplitude (nV)
Pulse Moment (A• ms)
B
Smooth and Blocky inversion
TDEM inversion
Water content (%)
Decay time (ms)
Resistivity (ohm-m)
Depth (m)
RMS=1.08%
C
QT inversion
PWC distribution(%)
Water content (%)
Geological column
Description
Depth (m)
Fine sand
Clay
Silt + Clay + Medium sand
Boulder Clay
Medium to coarse sand
Quartzite
Decay time (s)

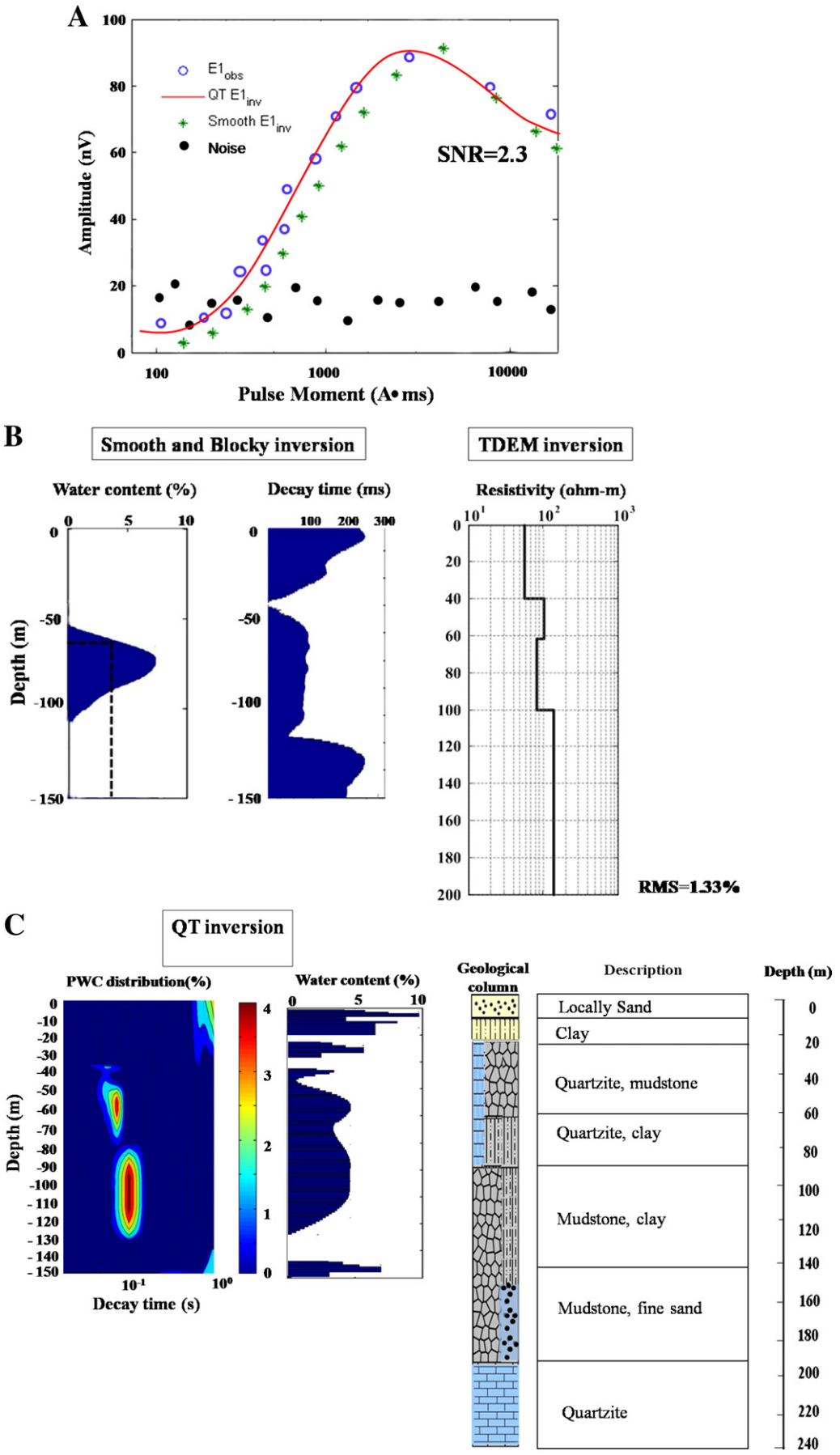
A
E1obs
QT E1inv
Smooth E1inv
Noise
SNR=2.3
Amplitude (nV)
Pulse Moment (A• ms)
B
Smooth and Blocky inversion
TDEM inversion
Water content (%)
Decay time (ms)
Resistivity (ohm-m)
Depth (m)
RMS=1.33%
C
QT inversion
PWC distribution(%)
Water content (%)
Decay time (s)
Geological column
Description
Depth (m)
Locally Sand
Clay
Quartzite, mudstone
Quartzite, clay
Mudstone, clay
Mudstone, fine sand
Quartzite

The QT inversion (QTI) developed by Mueller-Petke and Yaramanci (2010) was employed in the last step. This method consists of two parameters, the depth and the decay time T_2^*, and takes the MRS data set into account at one time. Additionally, employing multi-exponential inversion can considerably improve the correlation as it takes into account the signal superpositions of the MRS decay times from different layers and thus allows a better rendering of the high contrasts of the MRS decay time distributions in the subsurface.

5. Results of data interpretation

5.1. Seismic survey data

As displayed in Fig. 4A, Line SL-01 runs in the W–E direction and is approximately 1.5 km long. Boreholes BQ1 and BQ2 are located in the vicinity of the line and are marked above the seismic section.

The seismic section along line SL-01 shows a sequence of reflections at times of approximately 300 ms, corresponding to depths of 300–350 m. Several possible faults appear to intersect this reflection (between each set of colored lines). The seismic stack velocity decreases from over 1480 m/s on station a′ at the western edge of line SL-01 to less than 1270 m/s at station a′. This decreased velocity in the east may reflect increased amounts of fine sediment with increasing distance. The data from borehole BQ1 (Fig. 2) were used to determine the coherency of the seismic data. In addition to fault F1, F2, F3 and FF are possible faults along the survey line. The fault zone between d–d′ appears to have a large vertical displacement above the bedrock and less displacement along b–b′ and c–c′. However, none of the rest of the faults appears to extend to the surface, implying that only fault F1 has been active during the Quaternary. The fault F1 is then manifested on all of the seismic testing lines, which have been marked by yellow lines.

After an analysis of line SL-01, additional data were acquired along lines SL-02 and SL-03 (0.6 km long) to the north and south of line SL-01, respectively (Figs. 5 and 6). The major F1 faults are identified between CDPs e–e′ and g–g′. The locations of these faults were determined based primarily on the dramatic drop in the coherency of the reflected energy. Two minor faults F4 (f) and F5 (h–h′) are also identified. The geological units cannot be correlated to the seismic reflection data because of the lack of detailed subsurface information in the survey area.

The seismic line SL-04 was parallel to the other lines (Fig. 7A). The non-uniform reflections observed along the survey line at various points are most likely indication of faulting and folding. One of the most prominent features in the section is an anomalous zone, identified as F1 extension in the western part, between i–i′ (Fig. 7B). Additionally, we got the fault FF between k–k′ in the eastern part of the line. The zone laterally divides the section into separate parts with contrasting seismic characters. This disturbance zone may be related to a high-angle fault system intersected by the line. The reflectors are continuous on both sides of the zone and are clearly interrupted within the zone. Based on the assumption that the hydraulic conductivity of the groundwater formation is similar across the entire fracture zone, we proposed drilling borehole BQ3 within this zone. The lithological data from water well BQ3, located along line SL-04, are in agreement with the geological units and the top depth of the Bayanhua gravel inferred from the seismic reflection data. However, the aquifer has a yield of only 0.8 L/s, which falls short of the required water flow rate of 3 L/s. This result suggests that the permeabilities within the fault zones are not all satisfied, and further exploration was necessary to supplement our understanding gained from seismic reflection alone.

5.2. TDEM survey data

To select a more favorable site for a new borehole, the TDEM stations were established along the seismic lines SL01 (5 stations) and SL04 (9 stations), referred to as lines RL1 and RL2, respectively. Their locations are shown in Fig. 1. Compared to the seismic data, the profile of the TDEM apparent resistivity sounding curves better defines the interface between the upper resistive layers and the conductive layer, allowing for the identification of potential aquifers. However, the upper 10 m below the earth surface are recovered with less accuracy (Vouillamoz et al., 2002).

The pseudo-2D apparent resistivity for the cross-section at RL1 is correlated with the lithological units of borehole BQ1 (Fig. 8A). The interpreted resistivity can be divided into three groups:

1) Low resistivities (less than 115 Ω-m), characterized as mudstone (mainly clay) or clayey sand.
2) Moderate resistivities (115–130 Ω-m), typical for water-saturated aquifers and aquicludes.
3) High resistivities (greater than 130 Ω-m), typical for sandstone (mainly quartzite).

The RL2 line was superimposed with seismic line SL-04. As shown in Fig. 8B, the western part of RL2 indicates high resistivities from the depth of 40–280 m (soundings N_6, N_7). The models for the eastern part of the survey line (soundings N_{11}, N_{12}, and N_{13}) indicate an upper layer with low resistivities (approximately 90 Ω-m) to a depth of 150 m, followed by more resistive bedrock at 150–280 m deep (resistivity >130 Ω-m). The models for the center of the area show more variability. In general, a thin resistive layer (approximately 180 Ω-m) is followed by a conductive layer (80–180 m) with resistivities ranging from 115 to 130 Ω-m, which may correspond to a water-bearing stratum. In the deepest layer, the resistivity is greater than 130 Ω-m.

The results from the TDEM soundings N_7–N_9 in line RL2 indicate that the decreased resistivity in the shallow subsurface agrees well with the model obtained from the seismic data, which was interpreted as a saturated fracture zone (Fig. 7, i-i'). An agreement between the TDEM models and the seismic model was also observed at the eastern part of the line (under soundings N_{11}–N_{13}). The variations in both models fit the data well. This can be attributed to the presence of faults filled with groundwater. It should be emphasized that the TDEM data are consistent with both the independent seismic interpretation and the borehole BQ3 data. This borehole penetrates through the aquifer at a depth of 60–110 m, which is the minimum depth of the water-bearing strata along line RL2. According to this apparent resistivity profile, the location with the greatest measured depth to the aquifer roof rock was located approximately 100 m west of BQ3.

To select a site for a new borehole that would produce the desired flow rate, the final TDEM survey line RL3 was conducted based on BQ3 and located near and parallel to the lines RL2 and SL04 (Fig. 1). Fig. 8C shows the apparent resistivity profile RL3, including the N_{14}, N_{15}, N_{16}, N_{17}, N_{18}, N_{19}, N_{20}, N_{21}, N_{22}, and N_{23} soundings. As observed in the profile, there are 3 well-defined resistive layers. The first apparent resistivity layer is characterized by high values (shown in light blue) related to the sediments from the Cretaceous quartzite formation. The second layer is a ~200-m-thick conductive zone related to a saturated zone. This layer agrees with the information from a deep water well (BQ4) with a high rate of groundwater flow (>3.5 L/s).

Fig. 11. The MRS and TDEM inversion results at BQ3 site: (A) the measured MRS signal and calculated smooth inversion and QT model signals. SNR denotes signal to noise ratio; (B) Water content and decay time inverted by smooth and blocky inversion, as well as the TDEM inversion result at MRS sounding sites. (C) The QT inversion results and the nearby borehole data. PWC denotes partial water contents.

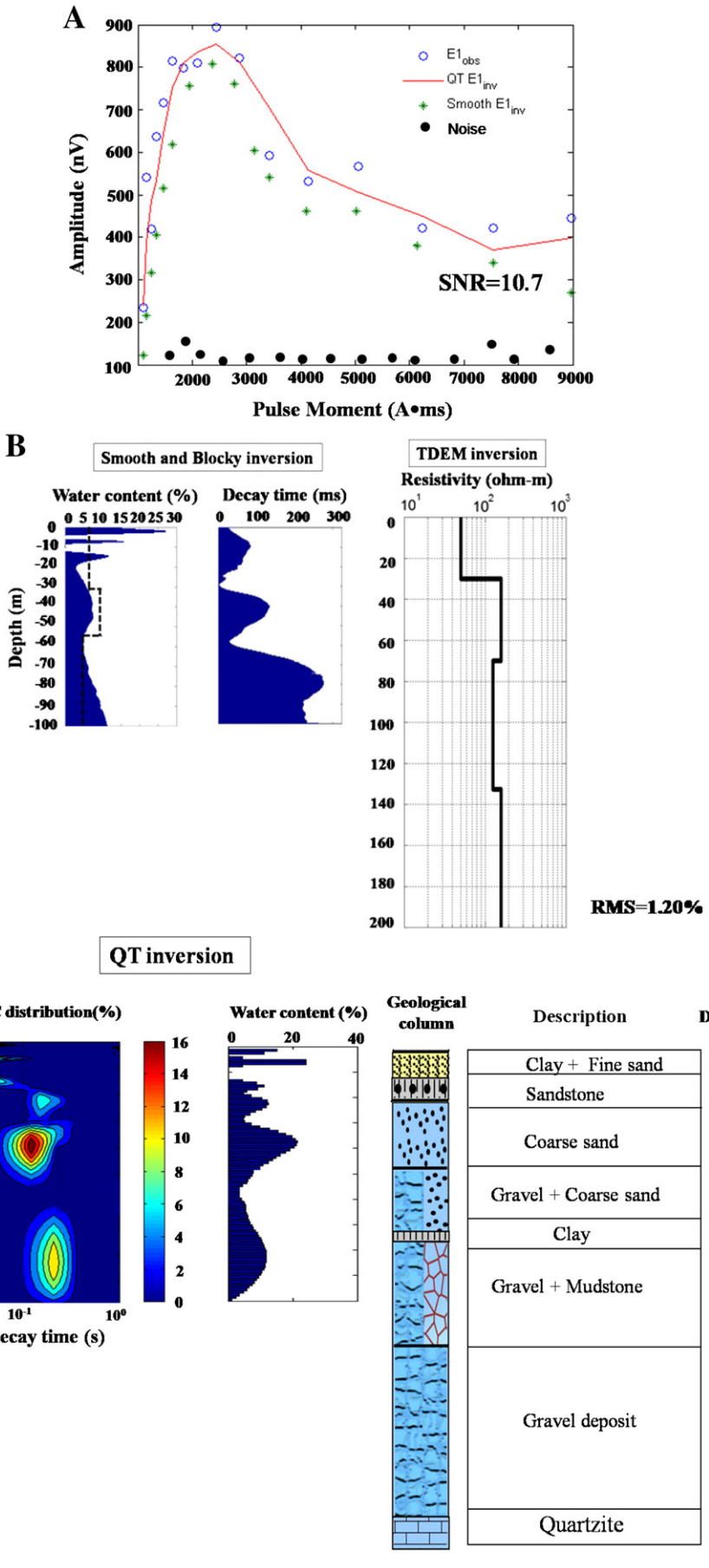
A
Amplitude (nV)
Pulse Moment (A•ms)
E1obs
QT E1inv
Smooth E1inv
Noise
SNR=10.7
B
Smooth and Blocky inversion
Water content (%)
Decay time (ms)
Depth (m)
TDEM inversion
Resistivity (ohm-m)
RMS=1.20%
C
QT inversion
PWC distribution(%)
Water content (%)
Depth (m)
Decay time (s)
Geological column
Description
Depth (m)
Clay + Fine sand
Sandstone
Coarse sand
Gravel + Coarse sand
Clay
Gravel + Mudstone
Gravel deposit
Quartzite

5.3. MRS related to hydrogeological parameters

For the MRS hydraulic conductivity and transmissivity estimation, calibration with boreholes is necessary. This calibration concerns mainly the local C_p factor calculation, which depends essentially on the reservoir's nature and structure. The product $w \times \Delta z$ is a more stable characteristic (Legchenko et al., 2004). Consequently, for MRS calibration it is more reliable to use the MRS estimates of transmissivity than of hydraulic conductivity. Thus, the MRS calibration, pumping tests from BQ1 to BQ4 were used.

A pumping test was performed close to MRS BQ1 station. The pumping test reveals an average transmissivity of 6.90×10^{-3} m^2/s. The MRS water content is approximately 20.1% (best fit model) and the MRS relaxation time, T_1, is 220 ms, which may correspond to medium sand (Legchenko et al., 2004).

A new borehole was then drilled near the MRS station BQ2. The transmissivity derived from the pumping test was estimated to be 8.81×10^{-3} m^2/s. The MRS water content was approximately about 23.25%, and the MRS relaxation time T_1 was approximately 420 ms, which may correspond to medium sand.

Following the above method, we obtain the following; T_{PT3} (BQ3) = 1.23×10^{-3} m^2/s, and T_{PT4} (BQ4) = 1.59×10^{-2} m^2/s. Subsequently, by using least-squares fitting, we obtained the best fit $C_p = 2.44 \times 10^{-8}$, This calibration constant can be used for these geological formations in the region. Furthermore, this best fit C_p achieves a mean difference of 12.29% for hydraulic conductivity and 26.81% for transmissibility (Fig. 9). After C_p calculation, T_{MRS} for the four boreholes were then estimated (as shown in Table 3).

In its technological state, the NUMIS system is designed for measurements with the range, $-1 \leq \Delta f\text{mean} \leq 1$ Hz, and corrections cannot be applied. Therefore, the frequency shift during all of the MRS measurements out of this range did not allow us to use this station for further calibration in several of the MRS stations (Table 4).

5.4. Integrated interpretation of MRS inversion and TDEM results 5.4.1 BQ2 sites

In BQ2, which is located in SL-01, the inversion is based on a good fit between the measured and the calculated data. The data quality was excellent because of very low noise conditions (Fig. 10A). As demonstrated in Fig. 10B, the smooth model of the subsurface water content and decay time indicates two dominating water-bearing layer: (1) from depths of approximately about 45.2–70.8 m with the decay time ranging between 70 and 112 ms, representing medium sand; the value of 72 Ω m of TDEM results suggested that conductive sediments might also exist; and (2) below 70.8 m, the water contents increase gradually and reach a maximum 22.1% at the depth of 91.6 m. As the decay time increases up to 180 ms, this layer may correspond to the water reservoir until the basement Bahuayan unit, in which the resistivity increases to 158 Ω m. Importantly, below the depth of 70 m, the water content and the decay time curves have a positive relationship, meaning that the increasing water content can be correlated with an increase in the pore size of the materials. The water table was also estimated by QT inversion (Fig. 10C). Consistent with the smooth inversion results, two groundwater layers were inverted. At the shallow depth, the aquifers show different relaxation times. In addition to the coarser material, the silt and boulder clay layers (<30 ms of dead time), which are represented with low water content because of the undetectable short decay times, are also estimated at the correct depth. Consistent with the smooth inversion, the deeper layer from 63.2 m to 90 m shows higher decay time. This result can be explained by a composition of the medium to coarse sand. The basement Bahuayan unit is in the TDEM data expressed by a 158 Ω m layer, for which the depth extension cannot be defined. And the bottom of the deeper aquifer here suggested by the MRS data is also possibly hosted in the basement Bahuayan unit.

5.4.1. BQ3 sites

Fig. 11A demonstrates the best fit between the measured MRS and the calculated data at BQ3. At shallow depths and pulse moments <800 Ams, the small signal amplitude was within the mean noise level. This means that the signal amplitudes produced by water are less than the noise level. However, the TDEM results indicate a relatively lower resistivity layer, which is 56 Ω m at approximate depths of about 0–40 m (Fig. 11B). Data with an interpretation consistent with a mixed material layer (mudstone, mainly clay), are also found in a borehole located near the measuring site. The resistivity has been increased to120 Ω m at an approximate depth of 40.1–62.0 m. This resistivity indicates increasing components of less conductive material, which have finally being correlated with quartzite from the borehole data. At the pulse moment >1000 Ams, the MRS signal is higher than the mean noise level, and the data are more reliable. From the result of smooth modeling, the subsurface one water-bearing layer is indicated at depths of 62.3–110.7 m. The water content here varies from 0.5% to 8.2%, in which the resistivity increases to 82 Ω m. At the depth from 100.6–150 m, a negative relationship between the water content and decay time is evident; i.e., the water content decreases sharply with increasing decay time. If the decay time T_2^* is reliable, this phenomenon may possibly occur in a sedimentary aquifer, which has a large mean pore size and high clay contents. However, as the TDEM inversion model expressed by a 140 Ω m, for which the MRS data could be possibly hosted in a basement limestone consisting of quartzite, mudstone and sandstone. We then considered that although the MRS data are more reliable at the pulse moment >1500 Ams, the low signal amplitude in the testing site BQ3 will affect the decay time estimation and T_2^* cannot be reliably interpreted. It should be emphasized that from the combined inversion of TDEM and MRS in the blocky model (black dotted line), the water content layer is consistent with the nearby borehole data. However, the QT inversions are not consistent with the borehole explanation at the shallow depth; the decay time is almost 1 s from 0 to 40 m. As the acquisition time of the NUMIS instrument was only 250 ms, the longer decay time was possibly an artifact, of the low signal to noise ratio. Therefore, the total water content in the QT inversion was derived from the summed overall decay times of PWC. The water contents at the shallow and deeper aquifers are greater than the smooth inversion results (Fig. 11C).

5.4.2. BQ4 sites

At the site of BQ4, the inversion obtained from the best fit between the measured and the calculated data is shown in Fig. 12A. Two shallow and one deeper water-bearing layers are indicated by the smooth inversion method (Fig. 12B). (1) At a very shallow depth, from approximately 0.5 to 4.0 m, the water content ranges from 5.0 to 26.4%, and T_2^* ranges from approximately 50 to 76 ms. As the survey was conducted immediately after the rainy season, this great water content seems logical for layers consisting of loose Quaternary eolian as well as sedimentary clay. Furthermore, the phenomenon may possible be correlated well with the TDEM data which indicate a relatively low resistivity layer (58 Ω m). (2) A second aquifer is indicated at a depth of approximately 7.3–9.7 m, where the water content varies from approximately 7.8% to 13.5%, with the T_2^* about 55–130 ms.

Fig. 12. The MRS and TDEM inversion results at BQ4 site: (A) The measured MRS signal and the calculated smooth inversion and QT model signals. SNR denotes signal to noise ratio; (B) Water content and decay time inverted by smooth and blocky inversions and the TDEM inversion result at the MRS sounding sites. (C) QT inversion results and the nearby borehole data. PWC denotes partial water contents.

This aquifer may be hosted in a coarse sand and sandstone with reference to the borehole data. For the TDEM model, this layer exhibits a resistivity of 76 Ω m, indicating a less conductive than that at shallow depths. (3) At depths from approximately 13.5 to 100.0 m, the water content varies from 4.6 to 21.0% whereas the decay time changes from 70 to 230 ms. Although the smooth and blocky inversions do not consider the deep aquifer separately, the longer decay time and water content may suggest a high content of coarse sand as well as gravel deposit. In comparison, this thin impermeable layer of clay at 60.7 to 65.2 m is correctly estimated by the QT inversion. As shown in Fig. 12C, the decay time of the different substructures exhibits different relaxation behaviors. Therefore, the layers from the top to the bottom show general trend of increasing decay time, most likely due to the coarser materials.

5.5. Identification and characterization of geological structures

Based on the above analysis, the geological cross sections determined along SL01 and SL04 in this area show the extension of the Bahuayan unit K_1b, and the Neogene formation in W–E directions (as shown in Fig. 13). New wells (ZK13, ZK14, ZK23, ZK24) were drilled by integrating the seismic data (Figs. 4 and 6) as well as MRS results (Site 44–Site50). In most parts, the K_1b unit holds not only coarser materials such as sand and gravel, but also finer sediments such as clay

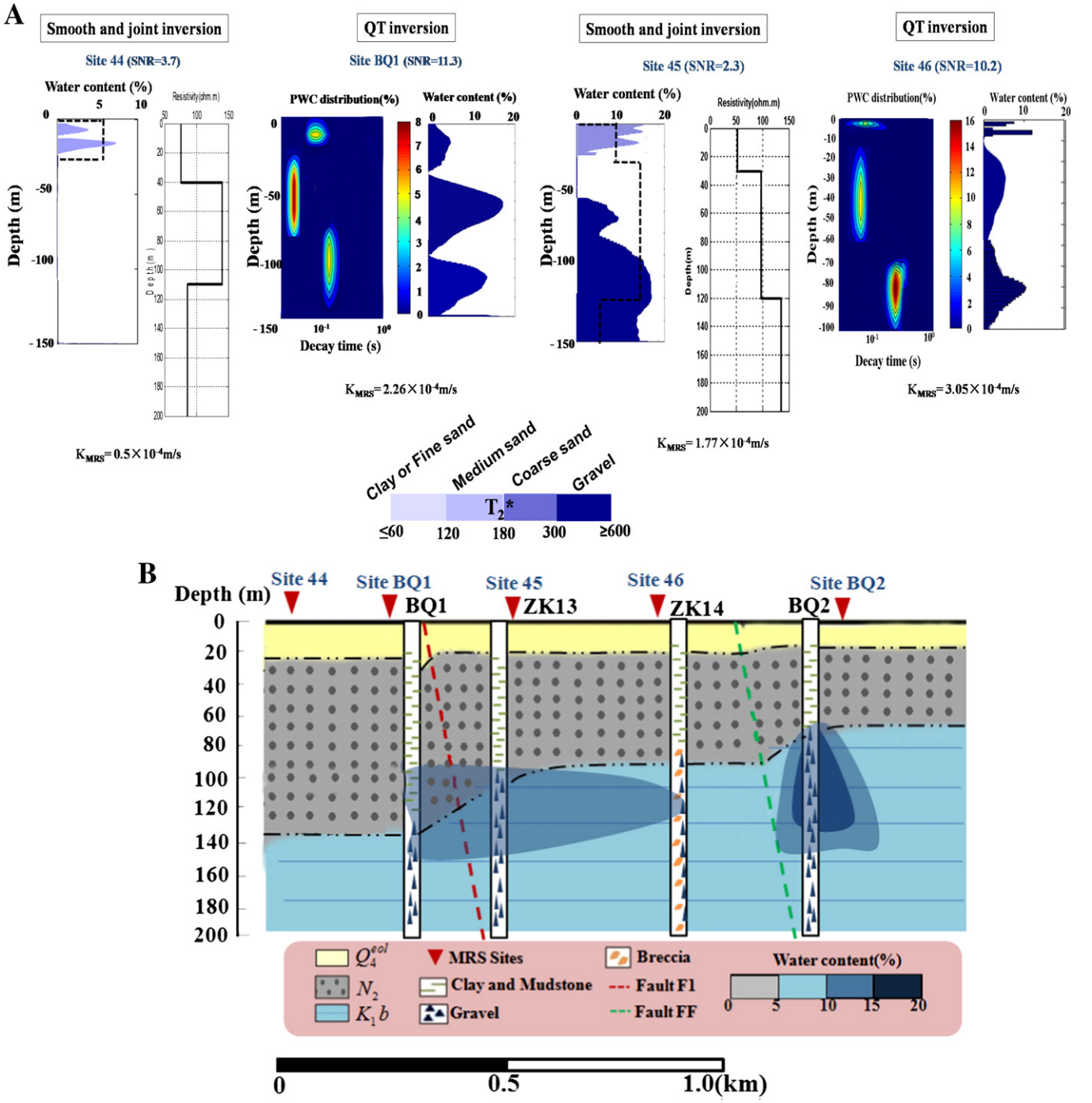

Fig. 13. A) Free water content, decay time and TEM models from MRS testing site 44, site BQ1, site 45 and site 46 in SL line 01. B) Interpolated cross-section of the MRS free water content [%] plotted on the geology.

and silt (ZK24). The Neogene formation N_2b, on the other hand, is mainly composed of clay and mudstone, with poor potential for hosting an aquifer. The MRS inversion schemes were chosen according to different signal-to-noise ratios. The joint inversion can correspond well with the water content distribution when the signal-to-noise ratio is relatively lower than 4.

In Fig. 13 (SL01 line), the cross-section with interpolated free water content illustrates the magnitude and position of the free water content distribution on the bottom of the N_2b unit and K_1b formation. The clay and mudstone of the N_2b unit are dominant in the upper part and the K_1b formation is the dominant stratigraphic unit in the lower part. In Fig. 14 (SL04 line), the thickness of the N_2b unit varies from 20 m to 160 m in the western part to approximately 25 to 40 m in the eastern part. The joint inversion and QT inversion schemes can identify one shallow aquifer in the Q_4 unit and one deeper aquifer in K_1b formation. The shallow aquifer usually starts a couple of meters below the surface with a maximum free water content of 3 to 6% down to a depth of 10 to 30 m. However, the deeper aquifer differs from site to site. According to the borehole data, it is located approximately 40 to 150 m in depth at the borehole site of ZK24. T_2^*-values range from 180 ms to 300 ms, which correspond to medium to coarse sands as supported by the borehole lithology. On the other hand, in site 47, basically no deeper water is found, indicating a more clayey material.

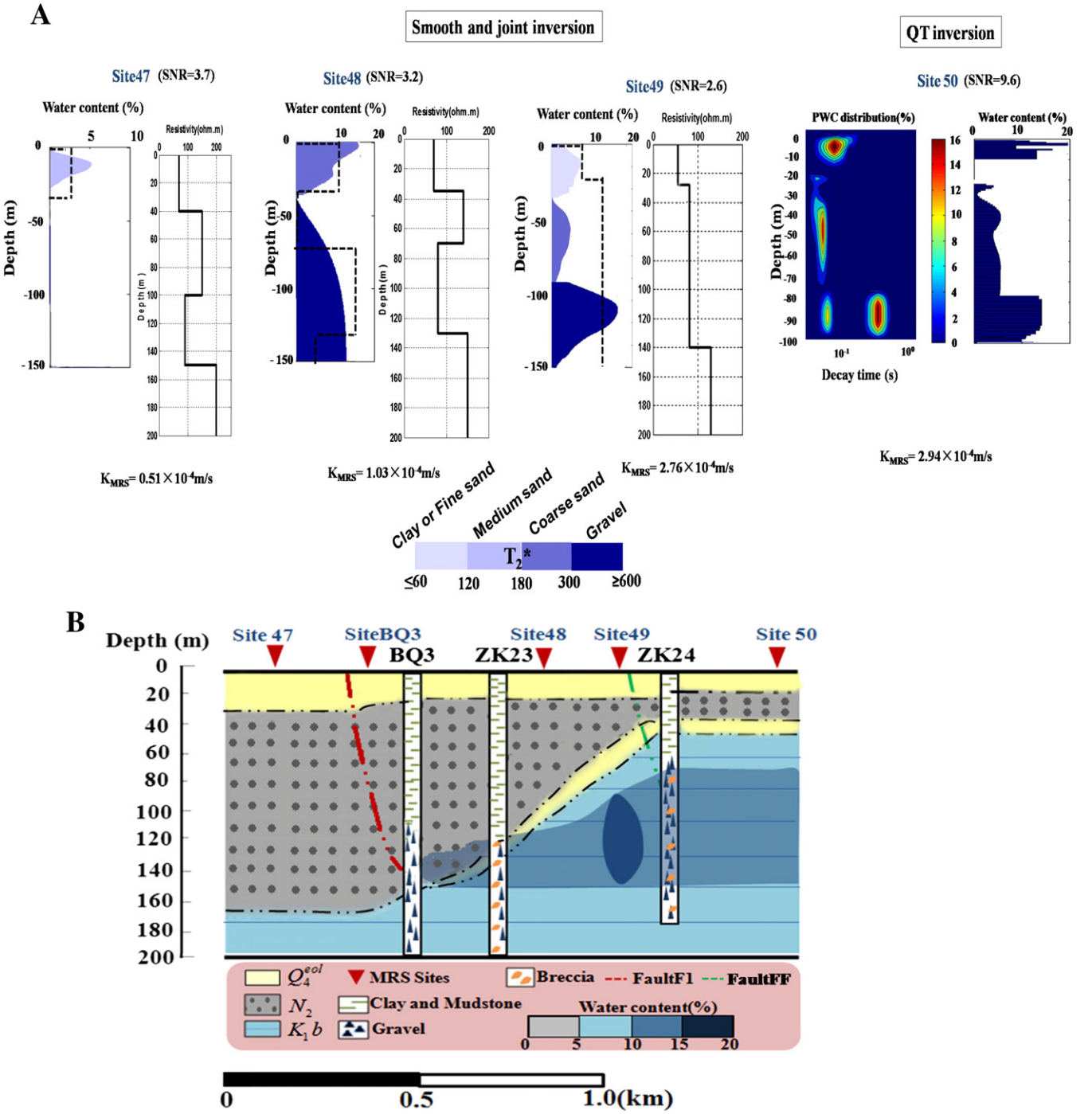

Fig. 14. A) Free water content, decay time and TEM models from the MRS testing site 47, site 48, site 49 and site 50 in SL line 04. B) Interpolated cross-section of MRS free water content [%] plotted over the geology.

6. Discussion

A fault zone can act as an important conduit rather than as a barrier for the groundwater flow if the following conditions are met. First, the permeability of the fault zone must be higher than that of the host rock. Second, the trend of the fault zone must be able to maximize its effect on the groundwater flow, preferably parallel to the hydraulic gradient (Babiker and Gudmundsson, 2004).

In this study, 2D seismic data allowed us to recognize and delineate the fault layer and its extension. In combination with the borehole data, it could reliably reveal the deep structure of the area and we could predict the boundary between the basement rocks and the overlying rocks. We then proposed the conceptual model for groundwater flow in the research area based on the effects of the major fault over the 3D maps (Fig. 15). We infer that the general hydraulic gradient follows the topography so that it trends sub-parallel with the main faults in the area. The major faults act as water conductors and transport groundwater to the discharge area. This model updates our understanding of fault distribution in this area. In addition to the orientation of F1 which can be speculated from the airborne electromagnetic, we also predict the presence of another fault FF, where the wells BQ2 and BQ4 are located.

The basement rocks were expected to be at a depth of 200 m at borehole BQ1 and a depth of 240 m at borehole BQ3. The site for the borehole BQ3 was decided upon, and drilled in 2002. However, the low yield of BQ3 (water yield of 0.8 L/s) revealed that the identification of the water bearing layer with the 2D seismic reflection method poses an important problem; that is, how to generate a proper geological model based on the correct velocity criterion. In addition to the equivalence data for interpretation, the labor and time costs can be significantly increased by adapting the 2D data acquisition and using wave sources.

The TDEM methods are very sensitive to the electrical conductivity of the aquifer. In our study, we have successfully recovered the fault strikes defined by the TDEM method using the apparent resistivity and indicated the potential extension of the aquifer in this area. For instance, with the TDEM method, borehole BQ3 was identified to penetrate through the thin aquifer at a depth of 60–110 m, which is the minimum depth of the water-bearing strata along line RL2. However, with the TDEM method alone, it is not possible to enhance the resolution of the thin layers (e.g. the impermeable layer), most likely because the objective layer is thin, compared to those above and below. The joint inversion of the seismic and resistivity data has also been reported in the literature (Dobroka et al., 1991). However, inherent ambiguities in the interpretation persist even after the combination of the data sets.

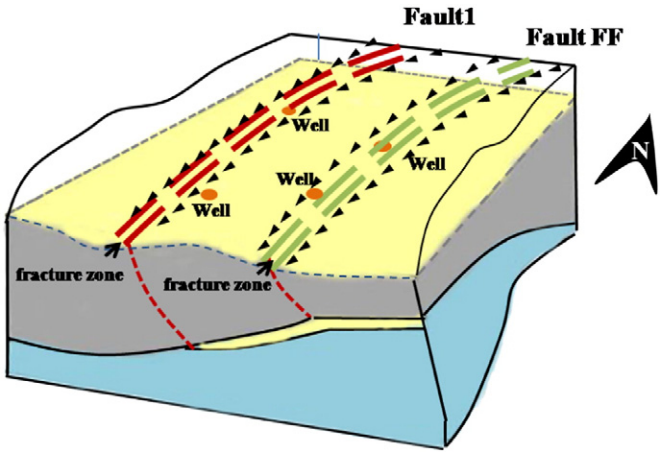

Fig. 15. The schematic presentation of the conceptual model of groundwater flow in the research area based on the derived geophysical models.

Although MRS could be used alone to determine the borehole locations (Vouillamoz et al., 2002), considering the complexity of faults, the use of several complementary geophysical techniques can increase success rate of borehole identification (Chalikakis et al., 2011). Therefore, we calculated the direct problem of TDEM for the three layer parameter models (BQ2) and four layer parameter models (BQ3 and BQ4), respectively. The MRS forward modeling for the calculation of the kernel function in the three inversion schemes were all based on the TDEM result, for the consideration of the conductive layer space rather than the homogeneous half-space (Braun and Yaramanci, 2011). Importantly, the blocky inversion constrained by the TDEM geometry does not always correspond to the MRS water content distribution, especially when the signal-to-noise ratio is low.

As the resistivities of the main water layer in the areas indicate moderate resistivity, both the inversion models identified the shallow and the deep aquifers and the accurate water content that is consistent with the geological structures. However, these conventional methods are impossible to enhance the resolution of the thin impermeable layers even being jointed used with the TDEM method. Thus, in our case, the state of the art inversion method of MRS, the QT inversion scheme was then used. It can directly provide both the water content and the decay-time depth distributions at once. As it uses the complete surface MRS data sets, the available information is then extracted with increased spatial resolution. Even the thin peat layer at approximately 4.5 m depth (BQ4) is significantly presented by this model of inversion. Additionally, as the decay time (T_2^*) was inverted by using multi-exponential fit, this inversion step is possible to provide the pore size distributions at the same water bearing layer. However, at noisier sites, and hence with more scattered field data, a joint inversion of MRS and TEM is usually more easily fitted to the data than the QT inversion.

Considering the fact that at the time of survey, only single-channel MRS is available, the combined geophysical techniques of TDEM, seismic and MRS were the best choice for water aquifer exploration, and proved to be very successful. Moreover, multi-channel data acquisition instruments and 2D and 3D numerical approaches are now more promising and may be better choices for hydrogeological investigations in faulted areas in the future (Jiang et al., 2011a,b; Walsh, 2008).

7. Conclusions

The physical conditions in the Baiqi, a rural area in the north of China, with small variations in the magnetic field, low magnetic susceptibility of the rocks and sediments and fairly low noise, make MRS a suitable method for groundwater exploration. However, the challenging problem is to identify valuable spots within a hydrogeological setting that is characterized by faults and fractures. Where the MRS is relatively limited for predicting the deep aquifers (>150 m), 2D seismic methods prove to be effective. A borehole was drilled, but it fell short of the required water flow rates.

The TDEM sounding allows the relative accurate identification of potential aquifers compared to using the 2D seismic alone. To further overcome the uncertainty of the TDEM interpretation, the MRS and TDEM together are evidenced to be useful for coupling water bearing layer thickness, especially when the MRS signal to noise ratio is low (Goldman et al., 1994; Legchenko et al., 2009). Moreover, the QT inversion, which uses the resistivity in the forward modeling, and the whole MRS data base for the inversion could help to distinguish the shallow impermeable layer from what could have been interpreted as water if only the smooth or block inversion had been carried out. Borehole drilling and pumping tests indicated that the conditions for these methods were favorable. The aquifer unit of interest was a Cretaceous Bahuayan units, characterized by medium resistivities and a lower velocity in comparison to the overlying rock.

References

Babiker, M., Gudmundsson, A., 2004. The effects of dykes and faults on groundwater flow in an arid land: the Red Sea Hills, Sudan. Journal of Hydrology 297 (1–4), 256–273.

Braun, M., Yaramanci, U., 2011. Evaluation of the influence of 2-D electrical resistivity on magnetic resonance sounding. Geophysics 16 (3), 95–103.

Burazer, M., Žitko, V., Radaković, D., Miodrag, P., 2010. Using geophysical methods to define the attitude and extension of water-bearing strata in the Miocene sediments of the Pannonian Basin. Journal of Applied Geophysics 72 (4), 242–253.

Chalikakis, K., Plagnes, V., Guerin, R., Valois, R., Bosch, F.P., 2011. Contribution of geophysical methods to karst-system exploration: an overview. Hydrogeology Journal 19 (6), 1169–1180.

Dobroka, M., Gyulai, A., Ormos, T., Csokas, J., Dresen, L., 1991. Joint inversion of seismic and geoelectric data recorded in an underground coal mine. Geophysical Prospecting 39, 643–665.

Fitterman, D.V., Steward, M.T., 1986. Transient electromagnetic sounding for groundwater. Geophysics 51, 995–1005.

Girard, J.F., Bouchera, M., Legchenko, A., Baltassata, J.M., 2007. 2D magnetic resonance tomography applied to karstic conduit imaging. Journal of Applied Geophysics 63 (3–4), 103–116.

Goldman, M., Rabinovich, B., Gilad, D., Gev, I., Schirov, M., 1994. Application of the integrated NMR–TDEM method in groundwater exploration in Israel. Journal of Applied Geophysics 31, 27–52.

Ji, Y.J., Lin, J., Cheng, D.F., Yu, S.B., 2003. Development and application of data processing software of ATEM-II transient electromagnetic instrument. Journal of Jilin University (Earth Science Edition) 33 (2), 242–245.

Ji, Y.J., Lin, J., Yu, S.B., Wang, Z., Wang, J., 2006. A study on solution of transient electromagnetic response during transmitting current turn-off in the ATTEM system. Chinese Journal of Geophysics 49 (6), 1884–1890.

Jiang, T., Lin, J., Li, T.L., Chen, Z.B., Zhang, L.H., 2006. Boosting signal to noise ratio of seismic signals using the phased-array vibrator system. Chinese Journal of Geophysics 49 (6), 1819–1825.

Jiang, C.D., Lin, J., Duan, Q.M., Sun, S.Q., Tian, B.F., 2011a. Statistical stacking and adaptive notch filter to remove high-level electromagnetic noise from MRS measurements. Near Surface Geophysics 9 (5), 459–468.

Jiang, C.D., Lin, J., Duan, Q.M., Tian, B.F., Hao, H.C., 2011b. A study on 2D magnetic resonance sounding with an array loop for groundwater exploration. Chinese Journal of Geophysics 54 (11), 2973–2983.

Kafri, U., Goldman, M., 2005. The use of the time domain electromagnetic method to delineate saline groundwater in granular and carbonate aquifers and to evaluate their porosity. Journal of Applied Geophysics 57 (3), 167–178.

Lachassagne, P., Baltassat, J.M., Legchenko, A., Machard de Gramont, H., 2005. The links between MRS parameters and the hydrogeological parameters. Near Surface Geophysics 3 (4), 259–265.

Legchenko, A., 2006. MRS measurements and inversion in presence of EM noise. 3rd Magnetic Resonance Sounding International Workshop. MRS 2006 Proceedings, Spain, Madrid, pp. 21–24.

Legchenko, A.V., Shushakov, O.A., 1998. Inversion of surface NMR data. Geophysics 63, 75–84.

Legchenko, A., Valla, P., 2002. A review of the basic principles for proton magnetic resonance sounding measurements. Journal of Applied Geophysics 50 (1–2), 3–19.

Legchenko, A., Baltassat, J.M., Bobachev, A., Martin, C., Robain, H., Vouillamoz, J.M., 2004. Magnetic resonance sounding applied to aquifer characterization. Ground Water 42 (3), 363–373.

Legchenko, A., Ezersky, M., Camerlynck, C., Al-Zoubi, A., Chalikakis, K., 2009. Joint use of TEM and MRS methods in a complex geological setting. Comptes Rendus Geosciences 341 (10–11), 908–917.

Liu, C.M., Xia, J., 2004. Water problems and hydrological research in the Yellow River and Huai and Hai River basins of China. Hydrological Processes 18 (12), 2197–2210.

Liu, H., Cai, X., Geng, L., Zhong, G., 2005. Restoration of pastureland ecosystems: a case study of western Inner Mongolia. Journal of Water Resources Planning and Management 131 (6), 420–430.

Liu, J.H., Liu, W., Li, L.J., Townley-Smith, L., Ren, T.Z., 2007. Effects of municipal solid waste compost on soil microbial populations and crop yields in saline–alkaline fields. Principles and Practices of Desertification I, 123–132.

Lubczynski, M., Roy, J., 2003. Hydrogeological interpretation and potential of the new magnetic resonance sounding (MRS) method. Journal of Hydrology 283 (1–4), 19–40.

Mohnke, O., Yaramanci, U., 2002. Smooth and block inversion of surface NMR amplitudes and decay times using simulated annealing. Journal of Applied Geophysics 50 (1–2), 163–177.

Mueller-Petke, M., Yaramanci, U., 2010. QT inversion—comprehensive use of the complete surface NMR data set. Geophysics 75, 199–209.

Myers, P.B., Miller, R.D., Steeples, D.W., 1987. Shallow seismic reflection profile of the Meers fault, Comanche County, Oklahoma. Geophysical Research Letters 15, 749–752.

Nielsen, M.R., Hagensen, T.F., Chalikakis, K., Legchenko, A., 2011. Comparison of transmissivities from MRS and pumping tests in Denmark. Near Surface Geophysics 9 (2), 211–223.

Plata, J., Rubio, F., 2002. MRS experiments in a noisy area of a detrital aquifer in the south of Spain. Journal of Applied Geophysics 50 (1–2), 83–84.

Porsani, J.L., Bortolozo, C.A., Almeida, E.R., Sobrinho, E.N.S., Santos, T.G.d., 2012. TDEM survey in urban environmental for hydrogeological study at USP campus in Sao Paulo City, Brazil. Journal of Applied Geophysics 76, 102–108.

Raiche, A.P., Jupp, D.L.B., Rutter, H., Vozoff, K., 1985. The joint use of coincident loop transient electromagnetic and Schlumberger sounding to resolve layered structures. Geophysics 50 (10), 1618–1627.

Schirov, M., Legchenko, A., Creer, G., 1991. A new direct noninvasive groundwater detection technology for Australia: exploration. Geophysics 22, 333–338.

Shtivelman, V., Goldman, M., 2000. Integration of shallow reflection seismics and time domain electromagnetics for detailed study of the coastal aquifer in the Nitzanim area of Israel. Journal of Applied Geophysics 44, 197–215.

Shtivelman, V., Frieslander, U., Zilberman, E., Amit, R., 1998. Mapping shallow faults at the Evrona playa site using high resolution reflection method. Geophysics 63, 1257–1264.

Vouillamoz, J.M., Descloitres, M., Bernard, J., Fourcassié, P., Romagny, L., 2002. Application of integrated magnetic resonance sounding and resistivity methods for borehole implementation, a case study in Cambodia. Journal of Applied Geophysics 50 (1–2), 67–81.

Walsh, D.O., 2008. Multi-channel surface NMR instrumentation and software for 1D/2D groundwater investigations. Journal of Applied Geophysics 66 (3–4), 140–150.

Yaramanci, U., 2004. New technologies in ground water exploration; surface nuclear magnetic resonance. Geologica Acta 2 (2), 109–120.

Yaramanci, U., Lange, G., Nodel, K., 1999. Surface NMR within a geophysical study of an aquifer at Haldensleben (Germany). Geophysical Prospecting 47 (6), 923–943.